Rapid structural change in low-lying states of neutron-rich Sr and Zr isotopes

H. Mei(梅花),[1,2] J. Xiang(向剑),[1] J. M. Yao(尧江明),[1,2,*] Z. P. Li(李志攀),[1] and J. Meng(孟杰)[3,4,5]

[1]*School of Physical Science and Technology, Southwest University, Chongqing 400715, China*

[2]*Physique Nucléaire Théorique, Université Libre de Bruxelles, C.P. 229, B-1050 Bruxelles, Belgium*

[3]*School of Physics, Peking University, Beijing 100871, China*

[4]*School of Physics and Nuclear Energy Engineering, Beihang University, Beijing 100191, China*

[5]*Department of Physics, University of Stellenbosch, Stellenbosch, South Africa*

(Received 17 January 2012; revised manuscript received 26 February 2012; published 20 March 2012)

The rapid structural change in low-lying collective excitation states of neutron-rich Sr and Zr isotopes is studied by solving a five-dimensional collective Hamiltonian with parameters determined from both relativistic mean-field and nonrelativistic Skyrme-Hartree-Fock calculations using the PC-PK1 and SLy4 forces, respectively. Pair correlations are treated in the BCS method with either a separable pairing force or a density-dependent zero-range force. The isotope shifts, excitation energies, and electric monopole and quadrupole transition strengths are calculated and compared with corresponding experimental data. The calculated results with both the PC-PK1 and the SLy4 forces exhibit a picture of spherical-oblate-prolate shape transition in neutron-rich Sr and Zr isotopes. However, compared with the experimental data, the PC-PK1 (or SLy4) force predicts a more moderate (or dramatic) change in most of the collective properties around $N = 60$. The underlying microscopic mechanism responsible for the rapid transition is discussed.

DOI: 10.1103/PhysRevC.85.034321 PACS number(s): 21.10.Re, 21.60.Jz, 27.60.+j

I. INTRODUCTION

The spectroscopy of nuclear low-lying states provides rich information about the interplay of nuclear collectivity and single-particle structure. For neutron-rich Sr and Zr isotopes, many spectroscopic data have been measured [1–10]. The abrupt change in the lifetimes and excitation energies of 2_1^+ states, two-neutron separation energies, and rms charge radii indicates a sudden onset of large quadrupole deformation at neutron number $N = 60$. In past decades, various models have been employed to study this dramatic transition in the low-energy structure of these nuclei [11–24], the description of which has been a challenge in theoretical nuclear physics.

Two main mechanisms based on shell models and mean-field approaches were proposed to explain the sudden onset of large nuclear collectivity at $N = 60$, namely, a strong isoscalar proton-neutron interaction between particles occupying the $g_{9/2}$-$g_{7/2}$ spin-orbit partners [11] and the occupation of low-K components of the $h_{11/2}$ neutron orbit [25,26], respectively. Besides these two factors, the simultaneous polarization of $2p_{1/2}$, $2p_{3/2}$, and $1f_{5/2}$ proton orbits as one goes from ^{96}Sr to ^{98}Sr and from ^{98}Zr to ^{100}Zr was pointed out to be the major factor in the more recent projected shell model study [27]. However, in most of the previous studies for nuclear low-lying states with, for instance the (projected) shell model, either a phenomenological effective interaction or effective charges for neutrons and protons defined within a specific valence space was introduced. In particular, it has been shown recently that large-scale shellmodel calculations with a more extended model space and carefully adjusted effective interaction are able to reproduce the low-spin spectroscopic data for $^{90-98}$Zr but fail to give large deformation properties for ^{100}Zr [28]. The mechanism responsible for the rapid transition in the structure of low-lying states in Sr and Zr isotopes around $N = 60$ requires further investigation.

Nuclear energy density functional theory (DFT) is nowadays one of the most important microscopic approaches for large-scale nuclear structure calculations in medium and heavy nuclei. The main ingredient of DFT is the energy density functional (EDF), which depends on densities and currents representing distributions of nucleonic matter, spins, momentum, and kinetic energy and their derivatives. In the past decades, much effort has been put into determining an EDF with reliable and good predictions by optimizing about 10 universal parameters to basic properties of nuclear matter and some selected nuclei. At present, there are three types of most successful EDFs, i.e., the non-relativistic Skyrme and Gogny forces and the effective relativistic Lagrangian, being employed extensively in the description of nuclear structure properties [29].

The nuclear DFT of a single-reference state (SR-DFT) with constraint on quadrupole moments, in the context of Hartree-Fock (HF) or Hartree-Fock-Bogoliubov (HFB) methods, has already been adopted to study the evolution of deformation energy surfaces in the β-γ plane (see the recent work [30]) for the neutron-rich Sr and Zr isotopes [26,31,32]. All of these studies have indeed shown increasing deformations based on the shift of the global minimum. However, most of these studies have focused on the properties of nuclear mean-field ground states. In particular, a competing weakly oblate deformed minimum coexisting with a large prolate one has been found in nuclei around $N = 60$, in which case the dynamic correlation effects from quadrupole fluctuation are expected to be significant. Moreover, the evolution behavior of low-lying excited states is sensitive to the balance between the oblate and the prolate minima. Therefore, it is necessary to extend these studies for the low-lying excited states in Sr and Zr isotopes.

*jmyao@swu.edu.cn

In the context of the generator-coordinate method (GCM), the framework of SR-DFT has been extended for studying nuclear low-lying states. In Ref. [33], the collective quadrupole and octupole excitations in Zr isotopes were studied using a basis generated by the HF + BCS calculations with the SkM* effective interaction. However, the low-lying states have not been described very well, probably owing to the absence of effects from triaxiality and angular momentum projections. In recent years, the GCM has been extended much farther by implementing the exact one-dimensional [34–36] or three-dimensional [37–40] angular momentum projection or together with particle number projection before or after variation for mean-field states in modern EDF calculations. Dynamic correlation effects related to symmetry restoration and quadrupole fluctuation (along both the β and γ the directions) around the mean-field minimum are included naturally without introducing any additional parameters. However, the application of these methods with triaxiality for systematic study is still very time-consuming. Up to now, this kind of study has been mostly restricted to light nuclei [41,42] and some specific medium-heavy nuclei [43,44].

As a Gaussian overlap approximation of the GCM, the collective Hamiltonian with parameters determined by self-consistent mean-field calculations is very simple in numerical calculations and has achieved great success in the description of nuclear low-lying states [45–49] and impurity effects of Λ hyperons in nuclear collective excitation [50]. In particular, a systematic study of low-lying states for a large set of even-even nuclei has been carried out with the Gogny D1S force mapped collective Hamiltonian, and good overall agreement with the low-lying spectroscopic data has been achieved [51]. However, some fine structures along the isotonic or isotopic chains are still not reproduced satisfactorily. For Sr and Zr isotopes, the evolution of isotope shifts and the change in the properties of low-lying states are found to be more moderate in comparison with the data. Therefore, in this work, we examine the evolution of low-lying states obtained from calculations with two other popular EDFs, i.e., the nonrelativistic Skyrme force and the effective relativistic Lagrangian. The difference in the results of these two calculations is emphasized.

The paper is organized as follows. In Sec. II we introduce briefly the method used to study low-lying states in neutron-rich Sr and Zr isotopes. The results and discussion are presented in Sec. III. A summary is reported in Sec. IV.

II. THE METHOD

The quantized five-dimensional collective Hamiltonian (5DCH) that describes the nuclear excitations of quadrupole vibration, rotation, and their couplings can be written in the form [45,46,48]

$$\hat{H} = \hat{T}_{\rm vib} + \hat{T}_{\rm rot} + V_{\rm coll}, \tag{1}$$

where $V_{\rm coll}$ is the collective potential. The vibrational kinetic energy reads

$$\hat{T}_{\rm vib} = -\frac{\hbar^2}{2\sqrt{wr}}\left\{\frac{1}{\beta^4}\left[\frac{\partial}{\partial\beta}\sqrt{\frac{r}{w}}\beta^4 B_{\gamma\gamma}\frac{\partial}{\partial\beta} - \frac{\partial}{\partial\beta}\sqrt{\frac{r}{w}}\beta^3 B_{\beta\gamma}\frac{\partial}{\partial\gamma}\right] + \frac{1}{\beta\sin 3\gamma}\left[-\frac{\partial}{\partial\gamma} \times \sqrt{\frac{r}{w}}\sin 3\gamma\, B_{\beta\gamma}\frac{\partial}{\partial\beta} + \frac{1}{\beta}\frac{\partial}{\partial\gamma}\sqrt{\frac{r}{w}}\sin 3\gamma\, B_{\beta\beta}\frac{\partial}{\partial\gamma}\right]\right\}, \tag{2}$$

and the rotational kinetic energy,

$$\hat{T}_{\rm rot} = \frac{1}{2}\sum_{k=1}^{3}\frac{\hat{J}_k^2}{\mathcal{I}_k}, \tag{3}$$

with $\hat{J}_k$ denoting the components of the angular momentum in the body-fixed frame of a nucleus. It is noted that the mass parameters $B_{\beta\beta}$, $B_{\beta\gamma}$, and $B_{\gamma\gamma}$, as well as the moments of inertia $\mathcal{I}_k$, depend on the quadrupole deformation variables β and γ,

$$\mathcal{I}_k = 4B_k\beta^2\sin^2(\gamma - 2k\pi/3), \quad k = 1, 2, 3. \tag{4}$$

Two additional quantities that appear in the expression for the vibrational energy, $r = B_1B_2B_3$ and $w = B_{\beta\beta}B_{\gamma\gamma} - B_{\beta\gamma}^2$, determine the volume element in the collective space. The corresponding eigenvalue problem is solved using an expansion of eigenfunctions in terms of a complete set of basis functions that depend on the deformation variables β and γ and the Euler angles ϕ, θ, and ψ [52].

The dynamics of the 5DCH is governed by the seven functions of the intrinsic deformations β and γ: the collective potential $V_{\rm coll}$, the three mass parameters, $B_{\beta\beta}$, $B_{\beta\gamma}$, and $B_{\gamma\gamma}$, and the three moments of inertia $\mathcal{I}_k$. These functions are determined by the relativistic mean-field (RMF) + BCS calculations using the PC-PK1 force [53] for the particle-hole (ph) and the separable pairing force (adjusted to reproduce the pairing properties of the Gogny force D1S in nuclear matter) [54,55] for the particle-particle (pp) channels or by the Skyrme-Hartree-Fock (SHF) + BCS calculations using the SLy4 force [56] for the ph channel and a density-dependent δ force for the pp channel,

$$V(\mathbf{r}_1, \mathbf{r}_2) = V_0^{\rm pp}\left[1 - \frac{\rho(\mathbf{r})}{\rho_0}\right]\delta(\mathbf{r}_1 - \mathbf{r}_2), \tag{5}$$

with a strength of $V_0^{\rm pp} = -1000\,{\rm MeV\,fm^3}$ and $\rho_0 = 0.16\,{\rm fm^{-3}}$ for both neutrons and protons and with a soft cutoff at 5 MeV above and below the Fermi energy as defined in Ref. [57]. A constraint on the deformation parameters of both β, ranging from 0 to 0.8 ($\Delta\beta = 0.05$), and γ, ranging from 0° to 60° ($\Delta\gamma = 6^\circ$), is imposed in both calculations.

The moments of inertia $\mathcal{I}_k$ are calculated using the Inglis-Belyaev formula [58,59]

$$\mathcal{I}_k = \sum_{i,j}\frac{(u_iv_j - v_iu_j)^2}{E_i + E_j}|\langle i|\hat{J}_k|j\rangle|^2, \tag{6}$$

where $k = 1, 2, 3$ denotes the axis of rotation, and the summation of i, j runs over the proton and neutron quasiparticle

states. The mass parameters $B_{\mu\nu}(\beta,\gamma)$ are given by [60]

$$B_{\mu\nu}(\beta,\gamma)=\frac{\hbar^2}{2}\left[\mathcal{M}_{(1)}^{-1}\mathcal{M}_{(3)}\mathcal{M}_{(1)}^{-1}\right]_{\mu\nu}, \tag{7}$$

with

$$\mathcal{M}_{(n),\mu\nu}(\beta,\gamma)=\sum_{i,j}\frac{\langle i|\hat{Q}_{2\mu}|j\rangle\langle j|\hat{Q}_{2\nu}|i\rangle}{(E_i+E_j)^n}(u_iv_j+v_iu_j)^2. \tag{8}$$

The mass parameters $B_{\mu\nu}$ in Eq. (7) can be converted into the forms of $B_{\beta\beta}$, $B_{\beta\gamma}$, $B_{\gamma\gamma}$ by using the relationships [52]

$$\begin{pmatrix}B_{\beta\beta}\\B_{\beta\gamma}\\B_{\gamma\gamma}\end{pmatrix}=\begin{pmatrix}\cos^2\gamma & \sin 2\gamma & \sin^2\gamma\\ -\frac{1}{2}\sin 2\gamma & \cos 2\gamma & \frac{1}{2}\sin^2\gamma\\ \sin^2\gamma & -\sin 2\gamma & \cos^2\gamma\end{pmatrix}\begin{pmatrix}B_{00}a_{00}\\B_{02}a_{02}\\B_{22}a_{22}\end{pmatrix}, \tag{9}$$

where the coefficients $a_{02}=a_{00}/\sqrt{a}_{22}=a_{00}/2$, with $a_{00}=9r_0^4A^{10/3}/16\pi^2$, and $r_0=1.2$.

The potential $V_{\rm coll}$ in Eq. (1) is given by

$$V_{\rm coll}(\beta,\gamma)=E_{\rm tot}(\beta,\gamma)-\Delta V_{\rm vib}(\beta,\gamma)-\Delta V_{\rm rot}(\beta,\gamma), \tag{10}$$

where $E_{\rm tot}$ is the standard nuclear total energy in the mean-field calculations with the nonrelativistic Skyrme force (cf. Eq. (1) in Ref. [61]) or the effective relativistic Lagrangian (cf. Eq. (9) in Ref. [38]), respectively. $\Delta V_{\rm vib}$ and $\Delta V_{\rm rot}$ are zero-point energies of vibrational and rotational motion,

$$\Delta V_{\rm vib}(\beta,\gamma)=\frac{1}{4}{\rm Tr}\left[\mathcal{M}_{(3)}^{-1}\mathcal{M}_{(2)}\right], \tag{11}$$

$$\Delta V_{\rm rot}(\beta,\gamma)=\sum_{\mu=-2,-1,1}\Delta V_{\mu\mu}(\beta,\gamma), \tag{12}$$

where the matrix $\mathcal{M}_{(n)}$ is determined by Eq. (8) with indices μ, ν running over 0 and 2 and corresponding mass quadrupole operators defined as $\hat{Q}_{20}\equiv 2z^2-x^2-y^2$ and $\hat{Q}_{22}\equiv x^2-y^2$. Moreover, $\Delta V_{\mu\mu}(\beta,\gamma)$ is calculated by

$$\Delta V_{\mu\nu}(\beta,\gamma)=\frac{1}{4}\frac{\mathcal{M}_{(2),\mu\nu}(\beta,\gamma)}{\mathcal{M}_{(3),\mu\nu}(\beta,\gamma)}, \tag{13}$$

where $\mathcal{M}_{(n),\mu\nu}(\beta,\gamma)$ is also determined by Eq. (8), but with the intrinsic components of the quadrupole operator defined as

$$\hat{Q}_{2\mu}\equiv\begin{cases}-2iyz, & \mu=1,\\ -2xz, & \mu=-1,\\ 2ixy, & \mu=-2.\end{cases} \tag{14}$$

Details of the solution of constrained RMF + BCS and SHF + BCS equations are given in Refs. [32,61], respectively.

III. RESULTS AND DISCUSSION

A. Collective parameters in the Hamiltonian

Figure 1 displays the moment of inertia along the x direction, mass parameters, and squared proton radii in 5DCH for ^{96,98,100}Sr and ^{98,100,102}Zr isotopes as functions of axial deformation parameter β determined from the mean-field calculations with both SLy4 and PC-PK1 forces. We note that the collective parameters in 5DCH do not change much in ^{96,98,100}Sr and ^{98,100,102}Zr isotopes in all the β-γ deformation regions, except for $B_{\beta\beta}$ with $\beta\simeq 0.4$ and $\gamma=60^\circ$ as well as $B_{\gamma\gamma}$ with $\beta\simeq 0.5$ and $\gamma=0^\circ$. In addition, the parameters in 5DCH determined from both SLy4 and PC-PK1 mean-field calculations are quite similar. But this is not really the case for the calculated collective potentials and we examine their differences in detail later. Moreover, for the mean squared proton radii r_p^2, the SLy4 predicts a slightly larger value than does the PC-PK1, by ∼0.5% systematically, which will definitely affect the absolute value of predicted nuclear charge radii.

B. Evolution of nuclear low-lying states

Figure 2 displays the electric quadrupole transition strength $B(E2;\,2_1^+\to 0_1^+)$, excitation energy $E_x(2_1^+)$ of the 2_1^+ state, and the ratio $R_{4/2}$ [$\equiv E_x(4_1^+)/E_x(2_1^+)$] as functions of neutron number in Sr and Zr isotopes from 5DCH calculations with both the SLy4 and the PC-PK1 forces. Systematically, the $B(E2;\,2_1^+\to 0_1^+)$ [or $E_x(2_1^+)$] values from the 5DCH calculations with both forces increase (or decrease) with the neutron number up to $N=62$ in both Sr and Zr isotopes, which indicates the existence of transition from spherical to prolate deformed shapes. However, compared with the experimental data, the evolution of $B(E2;\,2_1^+\to 0_1^+)$ and $R_{4/2}$ with respect to the neutron number around $N=60$ is much more dramatic (moderate) in the results of SLy4 (PC-PK1) calculations. Evolutionary behavior similar to that with the PC-PK1 force is also observed in the 5DCH calculations with the Gogny force D1S [51]. In particular, the dramatic decrease in $E_x(2_1^+)$ from $N=58$ to $N=60$ in Sr and Zr isotopes, together with the sudden increase in $E_x(2_1^+)$ in ^{96}Zr, is not reproduced in either calculation. Because the excitation energy is very sensitive to the moments of inertia, definitely much more effort should be devoted to determining these quantities precisely.

C. Deformation energy surfaces and collective wave functions

To understand the evolutionary character of spectroscopic quantities around $N=60$ shown in Fig. 2, we plot the deformation energy surfaces of ^{96,98,100}Sr and ^{98,100,102}Zr isotopes in the β-γ plane from the constrained mean-field calculations with both SLy4 and PC-PK1 forces in Figs. 3 and 4, respectively. In both calculations, there is always a weakly oblate deformed minimum coexisting with a prolate minimum in the deformation energy surfaces of ^{96,98,100}Sr and ^{98,100,102}Zr. Furthermore, the absolute minimum in both calculations is shifted from the oblate to the prolate side as the neutron number increases from $N=58$ to $N=60$. However, the subtle balance between these two minima is quite different in these two calculations, as shown in Fig. 5, where the total energy in ^{96,98,100}Sr and ^{98,100,102}Zr as a function of axial deformation parameter β is plotted. The evolution of deformation energy curves, i.e., from weakly oblate deformed ^{96}Sr and ^{98}Zr to large prolate deformed ^{98}Sr and ^{100}Zr in SLy4 calculations, is much more rapid than that in PC-PK1

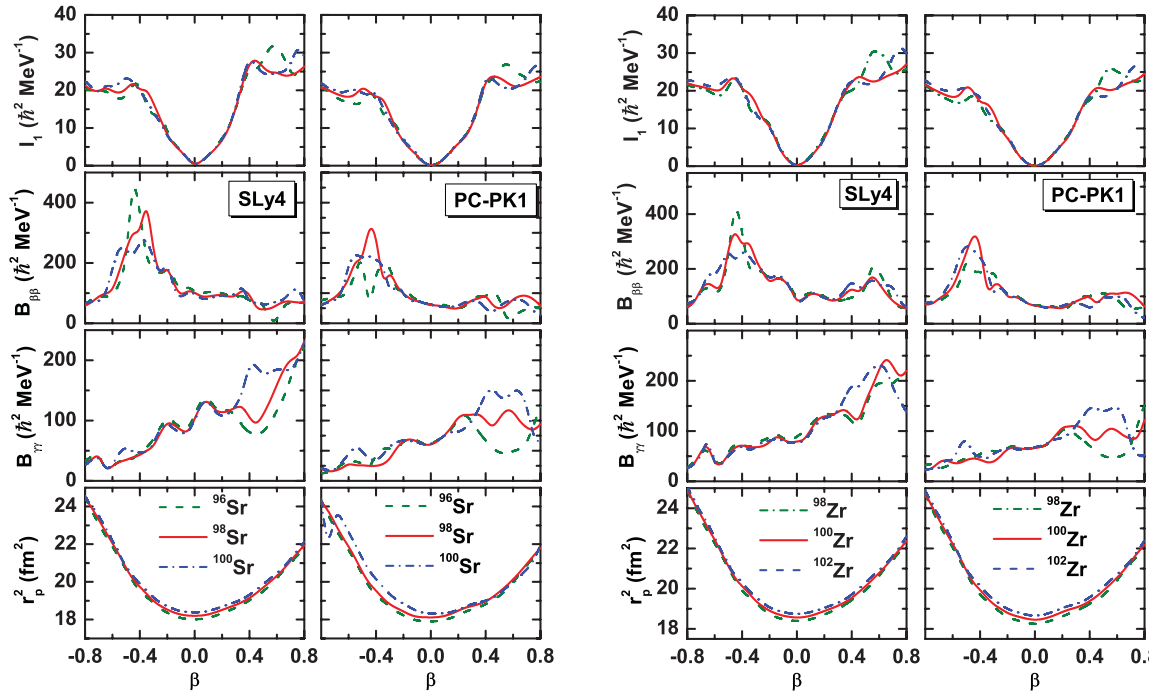

FIG. 1. (Color online) Moment of inertia along the x-direction I_1, mass parameters $B_{\beta\beta}$ and $B_{\gamma\gamma}$, and squared proton radii r_p^2 in 5DCH for ^{96,98,100}Sr (left) and ^{98,100,102}Zr (right) as functions of the axial deformation parameter β determined from the mean-field calculations with both the SLy4 and the PC-PK1 forces.

calculations. Moreover, the oblate and prolate minima in the deformation energy curves of ^{96,98,100}Sr and ^{98,100,102}Zr are quite close in energy. Very great mixing of oblate and prolate configurations is expected in their ground states. Contrary to the PC-PK1 calculations, the SLy4 force gives a broader or deeper oblate minimum in ^{96}Sr and ^{98}Zr, respectively, and a deeper or broader prolate minimum in ^{98,100}Sr and ^{100,102}Zr, respectively. In other words, ^{96}Sr and ^{98}Zr are more oblate, while ^{98,100}Sr and ^{100,102}Zr are more prolate, in the SLy4 calculations.

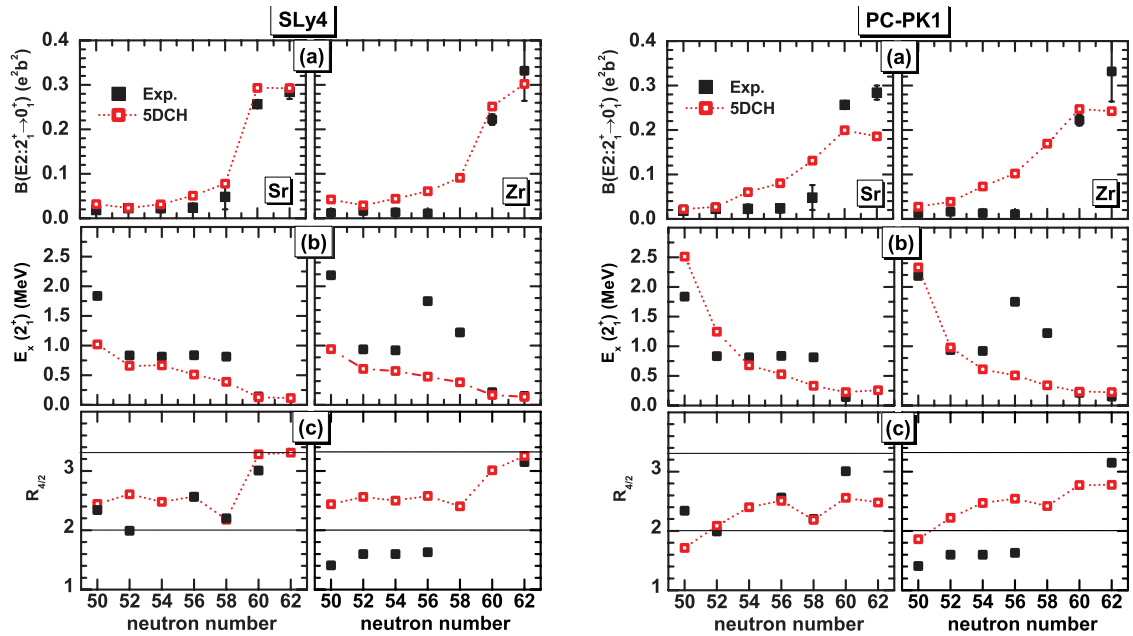

FIG. 2. (Color online) Electric quadrupole transition strength $B(E2; 2_1^+ \rightarrow 0_1^+)$, excitation energy $E_x(2_1^+)$, and ratio $R_{4/2}$ [$\equiv E_x(4_1^+)/E_x(2_1^+)$] as functions of neutron number in Sr and Zr isotopes from 5DCH calculations with the SLy4 force (left) and the PC-PK1 force (right), in comparison with the experimental data [62]. $R_{4/2}$ values for vibration (2.00) and rotation (3.33) limits are indicated by horizontal dotted lines.

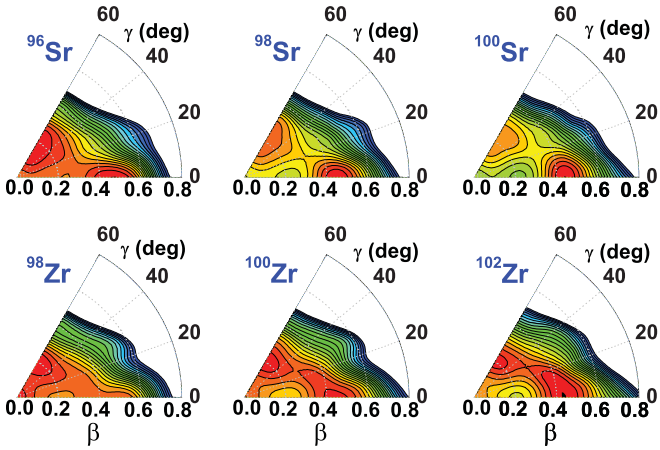

FIG. 3. (Color online) Total energy $E_{\rm tot}$ of ^{96,98,100}Sr and ^{98,100,102}Zr isotopes in the β-γ plane, from constrained SHF + BCS calculations with the SLy4 force for the ph channel and a density-dependent δ force for the pp channel. All energies are normalized to the absolute minimum. Each contour line is separated by 0.5 MeV.

The structural change in low-lying states is illustrated clearly in Fig. 6, where the distribution of squared collective wave functions $\rho_{I\alpha}$ in the β-γ plane for the 0_1^+ and 2_1^+ states from 5DCH calculations with both the SLy4 and the PC-PK1 forces is plotted. The $\rho_{I\alpha}$ is defined as

$$\rho_{I\alpha}(\beta,\gamma)=\sum_K \left|\Psi^I_{\alpha,K}(\beta,\gamma)\right|^2\beta^3|\sin 3\gamma|, \qquad (15)$$

which follows the normalization condition,

$$\int_0^\infty \beta d\beta \int_0^{2\pi} d\gamma \rho_{I\alpha}(\beta,\gamma)=1. \qquad (16)$$

Here, $\Psi^I_{\alpha,K}(\beta,\gamma)$ is the collective wave function that corresponds to the solution of 5DCH. The distributions of the squared collective wave functions in these two calculations are quite different. The SLy4 predicts a sudden transition from oblate ^{96}Sr to very good prolate ^{98,100}Sr, while the

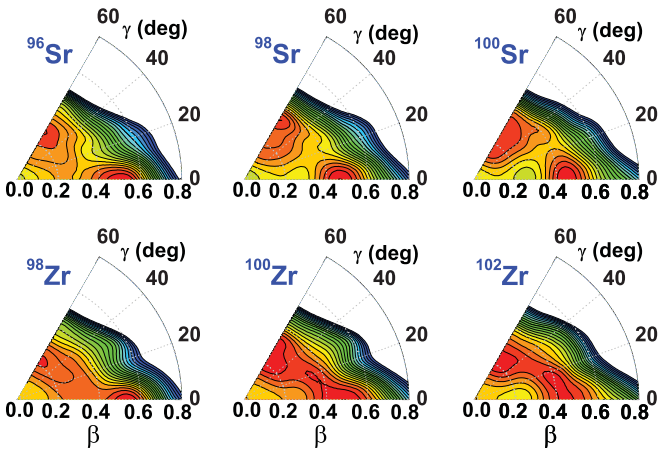

FIG. 4. (Color online) Same as Fig. 3, but from constrained RMF + BCS calculations with the PC-PK1 force for the ph channel and a separable force for the pp channel.

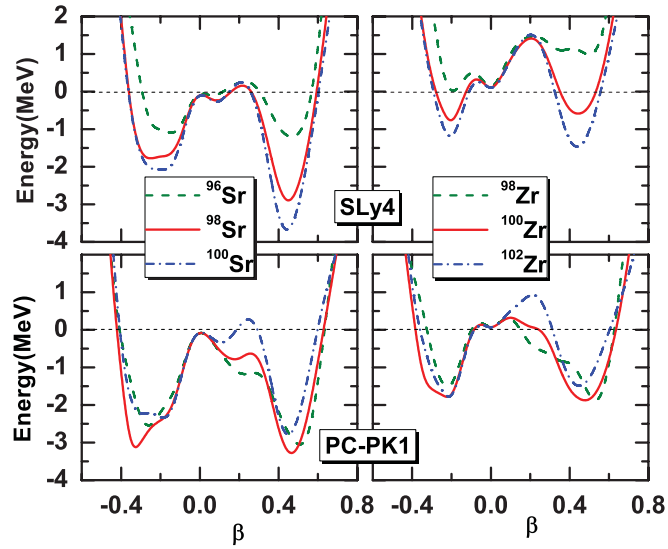

FIG. 5. (Color online) Total energy $E_{\rm tot}$ of ^{96,98,100}Sr and ^{98,100,102}Zr as a function of the axial deformation parameter β from constrained mean-field calculations with both the SLy4 and the PC-PK1 forces. All energies are normalized to the value at $\beta=0$.

PC-PK1 gives a coexistence picture for the ground states of ^{96,98,100}Sr, with the dominant component changing from oblate to prolate and back to oblate again moderately. For the 2_1^+ state in calculations with the SLy4 force, the dominant component in ^{96}Sr is oblate and it becomes well prolate in ^{98}Sr. However, in calculations with the PC-PK1 force, the dominant component is already prolate in ^{96}Sr. This picture provides an interpretation for the evolutionary character of $B(E2;\ 2_1^+\rightarrow 0_1^+)$, $E_x(2_1^+)$, and $R_{4/2}$ shown in Fig. 2. Compared with the experimental data for $B(E2;\ 2_1^+\rightarrow 0_1^+)$ and $R_{4/2}$, the SLy4 (or PC-PK1) force overestimates (or underestimates) somewhat the slope of the shape transition around $N=60$.

D. Isotope shifts and monopole transition

Nuclear charge radii or isotopic shifts are good indicators of shape changes along isotopic chains. In Refs. [31,32], the evolution of charge radii with the neutron number in Sr and Zr isotopes around $N=60$ was studied with the self-consistent constrained mean-field calculations. The charge radii corresponding to minima of different shapes in the deformation energy surface were compared with the data. It was shown that a rapid change in nuclear shape is essential to reproduce the experimental charge radii. However, in these two studies, the beyond-mean-field correlation effect on nuclear charge radii was not examined. In Ref. [63], the dynamic quadrupole correlation effect on charge radii of a large set of even-even nuclei was studied in the framework of configuration mixing of projected axially deformed states based on a topological Gaussian overlap approximation. It was shown that the dynamical correlation leads to an overall increase in radii, and it might also reduce the charge radii for some specific nuclei. Therefore, it is interesting to show the evolution of charge radii with the correlation effect from quadrupole fluctuation.

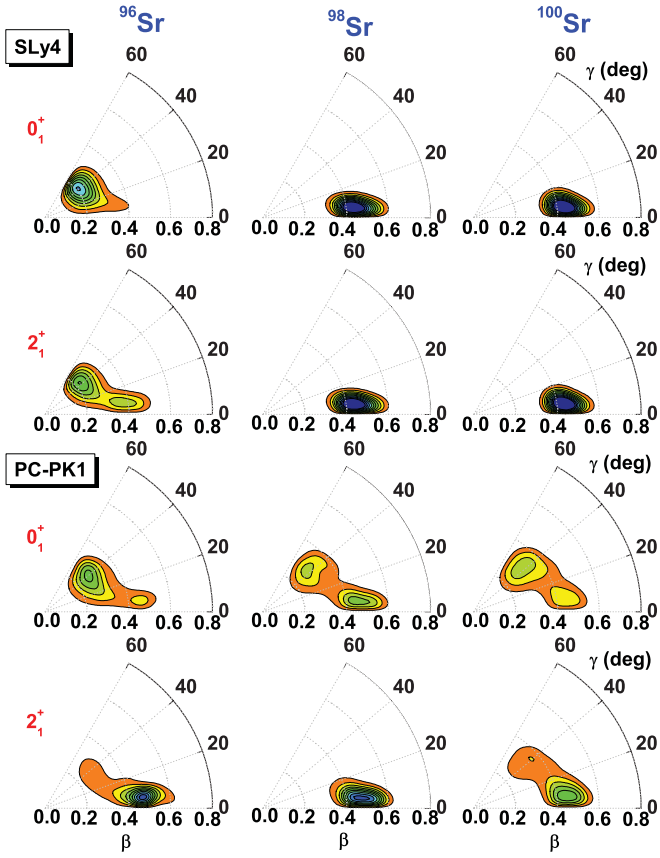

FIG. 6. (Color online) Distribution of squared collective wave functions in the β-γ plane for the 0_1^+ and 2_1^+ states in ^{96,98,100}Sr from 5DCH calculations with both the SLy4 and the PC-PK1 forces.

Figure 7 displays the isotope shifts corresponding to the configurations of prolate, oblate, and spherical minima in the deformation energy surfaces (shown in Figs. 3 and 4) for Sr and Zr isotopes from mean-field calculations with both SLy4 and PC-PK1 forces. In addition, we present the 5DCH predicted isotope shifts, in which the quadrupole fluctuation effect with triaxiality is included. It is shown clearly that the overall shape of isotope shifts is reproduced much better by 5DCH calculations with the dynamic correlation effect. In particular, the sudden rise in isotope shift from $N = 58$ to $N = 60$ is reproduced quite well in calculations with the SLy4 force, which can be understood from the changes, i.e., from predominantly oblate to prolate, in the corresponding collective wave function shown in Fig. 6. However, the PC-PK1 force predicts a quite smooth evolutionary trend for isotope shift, as expected from Fig. 6 as well. This shape evolution picture is consistent with that exhibited in other calculated quantities, such as $B(E2; 2_1^+ \rightarrow 0_1^+)$ and $R_{4/2}$.

Electric monopole transition strengths are a model-independent signature of the mixing of configurations with different mean-square charge radii [68] and therefore provide a good way to illustrate the occurrence of shape coexistence. Figure 8 shows the evolution of the electric monopole transition strength $\rho^2(E0; 0_2^+ \rightarrow 0_1^+)$ given by the off-diagonal

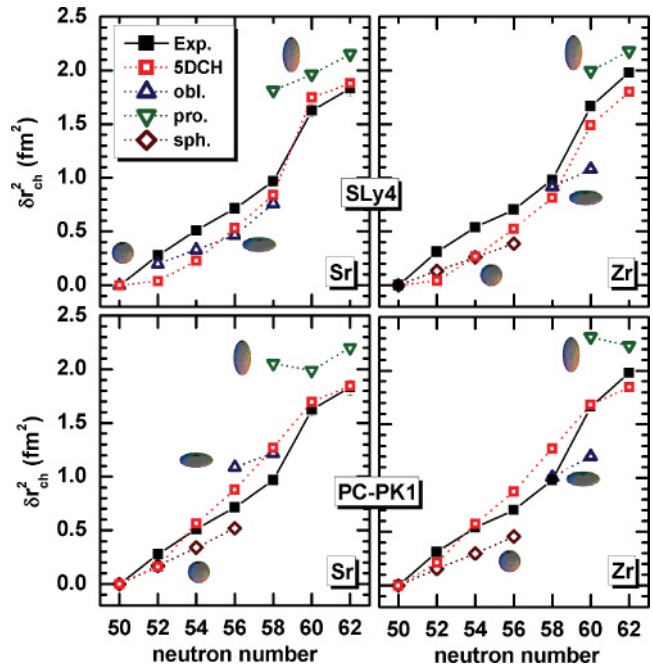

FIG. 7. (Color online) Isotope shifts (normalized to $N = 50$) corresponding, respectively, to configurations of prolate, oblate, and spherical minima in energy surfaces for Sr and Zr isotopes as a function of neutron number in SHF + BCS calculations with the SLy4 force and RMF + BCS calculations with the PC-PK1 force. Corresponding 5DCH calculated results and experimental data from Refs. [64,65] are given as well.

element of the charge radius,

$$\rho^2(E0; 0_2^+ \rightarrow 0_1^+) = \left| \frac{\langle 0_2^+ | \sum_k e_k r_k^2 | 0_1^+ \rangle}{e R_0^2} \right|^2, \qquad (17)$$

with $R_0 = 1.2A^{1/3}$ fm, with respect to the neutron number in neutron-rich Sr and Zr isotopes. The systematic increase in $\rho^2(E0: 0_2^+ \rightarrow 0_1^+)$ is similar in the calculations with the SLy4 and PC-PK1 forces. Both calculations predict the same peak position, i.e., at ^{96}Sr and ^{100}Zr, which are the nuclei before and after the dramatic transition, respectively. Quantitatively, however, as expected from the distribution of squared wave functions for ^{96,98,100}Sr in Fig. 6, the SLy4 (or PC-PK1) force predicts a much weaker (or stronger) mixing of oblate and prolate configurations in their ground states and, therefore, smaller (larger) $\rho^2(E0: 0_2^+ \rightarrow 0_1^+)$ values in ^{96,98,100}Sr. Compared with the experimental data for ^{98}Sr, the SLy4 (or PC-PK1) force underestimates (or overestimates) the $\rho^2(E0: 0_2^+ \rightarrow 0_1^+)$ value by a factor of approximately 2. Similar evolutionary behavior is also shown in Zr isotopes. However, except for ^{98}Zr, the difference in magnitude in the results of SLy4 versus PC-PK1 calculations is smaller than that in Sr isotopes.

Table I lists the calculated excitation energies $E_x(0_2^+)$ of 0_2^+ states in Sr and Zr isotopes with the SLy4 and PC-PK1 forces, in comparison with the available data. The predicted $E_x(0_2^+)$ from both calculations drops rapidly at $N = 58$ in both Sr and Zr isotopes. This behavior agrees with the data for Zr

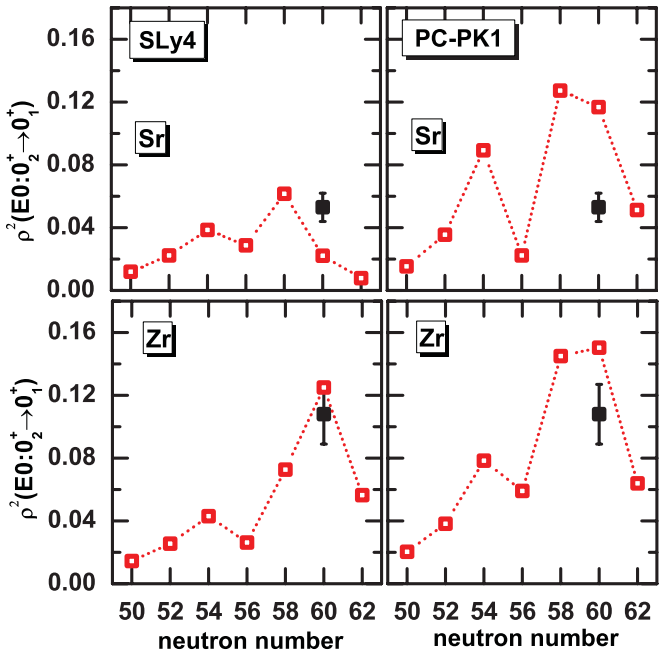

FIG. 8. (Color online) Electric monopole transition strength $\rho^2(E0;\ 0_2^+ \to 0_1^+)$ from 5DCH calculations with both SLy4 and PC-PK1 forces, in comparison with experimental data [66,67].

isotopes, but it is two neutrons earlier for Sr isotopes, where the experimental $E_x(0_2^+)$ decreases dramatically at $N = 60$.

E. Single-particle energy levels and spin-orbit splitting

Nuclear low-lying states reflect information about the underlying single-particle structure, and vice versa. Therefore, to understand the evolutionary character of collectivity in Sr and Zr isotopes around $N = 60$ in calculations with both SLy4 and PC-PK1 forces, in Fig. 9, we plot the neutron and proton single-particle energy levels in ^{96,98}Sr as functions of the axial deformation parameter β. In general, the minima in the deformation energy curve are associated with a shell effect owing to the low level density around the Fermi energy. It is shown in Fig. 9 that, for the proton single-particle energy levels, both calculations predict a large shell gap around the Fermi energy level on the prolate side, which is mainly formed by two levels split from the degenerate $\pi 1g_{9/2}$ state owing to the deformation (or Jahn-Teller) effect. The size of this energy gap does not change very much from ^{96}Sr to ^{98}Sr in both calculations. This means that the proton plays a minor role in the rapid nuclear shape transition from the mean-field point of view. For the neutron single-particle energy levels, both calculations predict two evident shell gaps around the Fermi energy level on the oblate and prolate sides, however, the details of the single-particle structure are quite different.

TABLE I. Calculated excitation energies (in MeV) of 0_2^+ states in Sr and Zr isotopes with the SLy4 and PC-PK1 forces, in comparison with the available data [62].

N	Sr			Zr		
	SLy4	PC-PK1	Expt.	SLy4	PC-PK1	Expt.
50	2.181	2.938	3.152	2.178	3.095	1.761
52	1.742	1.566	(2.674)	1.773	1.765	1.383
54	1.198	1.340	2.088	1.329	1.620	1.300
56	1.149	1.005		1.204	1.273	1.582
58	0.440	0.327	1.229	0.596	0.506	0.854
60	0.590	0.216	0.215	0.414	0.468	0.331
62	0.907	0.313	(0.938)	0.724	0.593	(0.895)

Compared with the PC-PK1 force, the SLy4 force predicts a stronger spin-orbit splitting for neutrons (by a factor of $\sim$1.1) for all states, as shown in Fig. 10, where the splitting of neutron spin-orbit doublet states,

$$\Delta E_{\rm so} = \frac{\epsilon_{nlj_>} - \epsilon_{nlj_<}}{2\ell + 1}, \quad j_{\gtrless} = \ell \pm 1/2, \tag{18}$$

in the spherical states of ^{96}Sr and ^{98}Sr as a function of the orbital angular momentum ℓ is plotted. $\epsilon_{nlj_<}$ is the energy of the single-particle state with quantum numbers $(n, \ell, j_<)$. Consequently, the position of the $\nu 1g_{7/2}$ state is pushed up and that of the $\nu 1h_{11/2}$ state is pulled down compared with the PC-PK1 results as shown in Fig. 9. As a result, the shell gaps around the Fermi energy at the spherical point and the minima of the deformation energy curves are quite different. For the spherical point ($\beta = 0$), a relatively large shell gap at $N = 56$, which provides a mechanism responsible for the observed much higher $E_x(2_1^+)$ in ^{96}Zr, is shown in the SLy4 calculation but not in the PC-PK1 calculations. Moreover, compared with the PC-PK1 results for ^{96}Sr, the position of the $\nu 2d_{5/2}$ state is almost the same, but the $\nu 1h_{11/2}$ state is much lower in the SLy4 results. As a result, the shell gap around the Fermi level on the prolate side, mainly formed by the $K = 3/2$ component of the $\nu 2d_{5/2}$ orbit, the intruded $K = 1/2$ component of the $\nu 2f_{7/2}$ orbit, and the other two levels with $K = 3/2,\ 5/2$ split from the $\nu 1h_{11/2}$ orbit, is much smaller than that in the PC-PK1 calculations. In ^{98}Sr, the energy of the $\nu 1h_{11/2}$ state is shifted up, which broadens the shell gap significantly on the prolate side. This big change in the energy gap around the Fermi energy is responsible for the sudden onset of the large prolate deformation at $N = 60$ given by the SLy4 calculations. In the PC-PK1 calculations, however, this change in the shell gap on the prolate side is more moderate. We note that, similarly to the PC-PK1 results, the shift of the $\nu 1h_{11/2}$ state in ^{96,98}Sr from the Gogny D1S calculations is small and the change in the shell gap on the prolate side is not significant [69]. On the other hand, compared with the SLy4 force, the PC-PK1 predicts a larger shell gap on the oblate side of ^{96,98}Sr, which provides the mechanism responsible for the strong mixing of prolate and oblate shapes in their ground states.

IV. SUMMARY

In summary, the rapid structural change in low-lying collective excitation states of neutron-rich Sr and Zr isotopes has been studied by solving a 5DCH with parameters determined from both RMF and SHF calculations. Pair correlations are

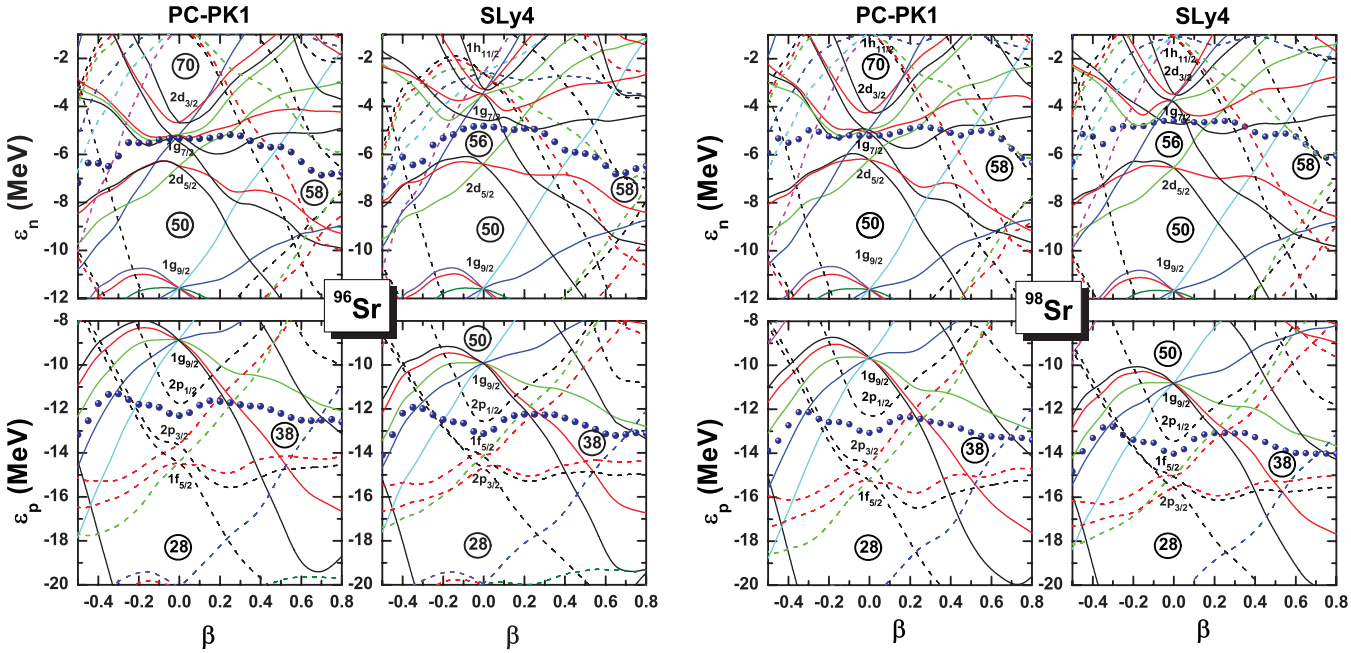

FIG. 9. (Color online) Neutron and proton single-particle energy levels in ^{96}Sr (left) and ^{98}Sr (right) from the constrained mean-field calculations with both SLy4 and PC-PK1 forces. Circles denote the corresponding Fermi energy levels.

treated in the BCS method with either a separable pairing force or a density-dependent zero-range force. The isotope shifts, excitation energies, and electric monopole and quadrupole transition strengths have been calculated and compared with corresponding experimental data. The calculated results with both the PC-PK1 and the SLy4 forces exhibit a picture of spherical-oblate-prolate shape transition in neutron-rich Sr and Zr isotopes. However, compared with the experimental data, the PC-PK1 (or SLy4) force predicts a more moderate (or dramatic) change in most of the collective properties around $N = 60$ and a much stronger (or weaker) mixing between oblate and prolate configurations in their ground states. The difference between these two calculations is mainly because of the quite different structure in neutron single-particle states, mostly caused by the different spin-orbit interaction strengths. Moreover, the sudden broadening of the neutron shell gap on the prolate side, mainly formed by the $K = 3/2$ component of $\nu 2d_{5/2}$, the intruded $K = 1/2$ component of $\nu 2f_{7/2}$, and the other two components of the $\nu 1h_{11/2}$ state, has been shown to be responsible for the rapid shape transition at $N = 60$. However, it must be pointed out that the rapid change in the excitation energy of the first 2^+ state has not been reproduced in calculations with both the PC-PK1 and the SLy4 forces. In particular, even though the SHF + BCS calculation with the SLy4 force indeed predicts a sizable spherical shell gap at $N = 56$, the corresponding 5DCH calculation is not able to reproduce the suddenly increased excitation energy for the first 2^+ state at ^{96}Zr. A further, beyond-mean-field investigation is required.

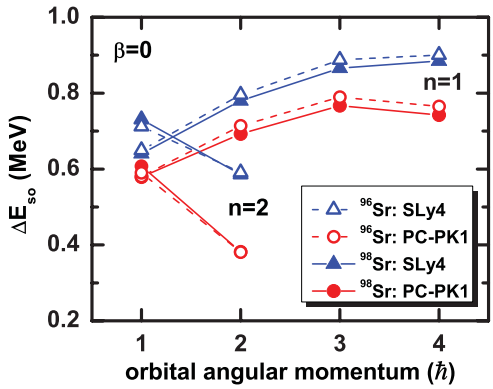

FIG. 10. (Color online) Splitting of neutron spin-orbit doublet states [cf. Eq. (18)] in the spherical states of ^{96}Sr (open symbols) and ^{98}Sr (filled symbols) as a function of the orbital angular momentum ℓ from mean-field calculations with both the SLy4 (triangles) and the PC-PK1 (circles) forces.

ACKNOWLEDGMENTS

J.M.Y. acknowledges fruitful discussions with Paul-Henri Heenen. This work was partly supported by Major State Basic Research Development Program 2007 CB815000, the National Science Foundation of China under Grant Nos. 11105111, 11105110, 11175002, 10975008, and 10947013, Fundamental Research Funds for the Central Universities (Grant Nos. XDJK2010B007 and XDJK2011B002), the Research Fund for the Doctoral Program of Higher Education under Grant No. 20110001110087, and Southwest University Initial Research Foundation Grants to Doctors (Nos. SWU109011 and SWU110039).

[1] G. Jung, B. Pfeiffer, L. J. Alquist, H. Wollnik, P. Hungerford, S. M. Scott, and W. D. Hamilton, Phys. Rev. C **22**, 252 (1980).
[2] F. Schussler, J. A. Pinston, B. Monnand, and A. Moussa, Nucl. Phys. A **339**, 415 (1980).
[3] K. Kawade *et al.*, Z. Phys. A **304**, 293 (1982).
[4] J. Eberth and K. Sistemich (eds.), *Nuclear Structure of the Zirconium Region*, Proceedings of the International Workshop (Springer-Verlag, Berlin, 1988).
[5] H. Mach *et al.*, Phys. Lett. B **230**, 21 (1989).
[6] H. Mach *et al.*, Nucl. Phys. A **523**, 197 (1991).
[7] G. Lhersonneau *et al.*, Phys. Rev. C **49**, 1379 (1994).
[8] W. Urban *et al.*, Nucl. Phys. A **689**, 605 (2001).
[9] U. Hager *et al.*, Phys. Rev. Lett. **96**, 042504 (2006).
[10] C. Goodin *et al.*, Nucl. Phys. A **787**, 231 (2007).
[11] P. Federman and S. Pittel, Phys. Lett. B **77**, 29 (1978); Phys. Rev. C **20**, 820 (1979).
[12] A. Kumar and M. R. Gunye, Phys. Rev. C **32**, 2116 (1985).
[13] D. Galeriu, D. Bucurescu, and M. Ivaqcu, J. Phys. G **12**, 329 (1986).
[14] S. Michiaki and A. Akito, Nucl. Phys. A **515**, 77 (1990).
[15] P. Möler, J. R. Nix, W. D. Myers, and W. J. Swiatecki, At. Data Nucl. Data Tables **59**, 185 (1995).
[16] J. Skalski, S. Mizutori, and W. Nazarewicz, Nucl. Phys. A **617**, 282 (1997).
[17] G. A. Lalazissis, S. Raman, and P. Ring, At. Data Nucl. Data Tables **71**, 1 (1999).
[18] A. Holt, T. Engeland, M. Hjorth-Jensen, and E. Osnes, Phys. Rev. C **61**, 064318 (2000)
[19] F. R. Xu, P. M. Walker, and R. Wyss, Phys. Rev. C **65**, 021303(R) (2002).
[20] J. García-Ramos, K. Heyde, R. Fossion, V. Hellemans, and S. De Baerdemacker, Eur. Phys. J. A **26**, 221 (2005).
[21] L. S. Geng, H. Toki, and J. Meng, Prog. Theor. Phys. **113**, 785 (2005).
[22] S. Lalkovski and P. Van Isacker, Phys. Rev. C **79**, 044307 (2009).
[23] P. Van Isacker, A. Bouldjedri and S. Zerguine, Nucl. Phys. A **836**, 225 (2010).
[24] M. Böyükata, P. Van Isacker, and I. Uluer, J. Phys. G **37**, 105102 (2010).
[25] T. R. Werner, J. Dobaczewski, M. W. Guidry, W. Nazarewicz, and J. A. Sheikh, Nucl. Phys. A **578**, 1 (1994).
[26] P. Bonche, H. Flocard, P. H. Heenen, S. J. Krieger, and M. S. Weiss, Nucl. Phys. A **443**, 39 (1985).
[27] S. Verma, P. A. Dar, and R. Devi, Phys. Rev. C **77**, 024308 (2008).
[28] K. Sieja, F. Nowacki, K. Langanke, and G. Martínez-Pinedo, Phys. Rev. C **79**, 064310 (2009).
[29] G. A. Lalazissis, P. Ring, and D. Vretenar (eds.), *Extended Density Functionals in Nuclear Structure Physics,* Lecture Notes in Physics 641 (Springer, Heidelberg 2004).
[30] B.-N. Lu, E.-G. Zhao, and S.-G. Zhou, Phys. Rev. C **84**, 014328 (2011).
[31] R. Rodríguez-Guzmán, P. Sarriguren, L. M. Robledo, and S. Perez-Martin, Phys. Lett. B **691**, 202 (2010).
[32] J. Xiang, Z. P. Li, Z. X. Li, J. M. Yao, and J. Meng, Nucl. Phys. A **873**, 1 (2012).
[33] J. Skalski, P.-H. Heenen, and P. Bonche, Nucl. Phys. A **559**, 221 (1993).
[34] A. Valor, P. H. Heenen, and P. Bonche, Nucl. Phys. A **671**, 145 (2000).
[35] R. Rodríguez-Guzmán, J. L. Egido, and L. M. Robledo, Nucl. Phys. A **709**, 201 (2002).
[36] T. Nikšić, D. Vretenar, and P. Ring, Phys. Rev. C **73**, 034308 (2006); **74**, 064309 (2006).
[37] M. Bender and P.-H. Heenen, Phys. Rev. C **78**, 024309 (2008).
[38] J. M. Yao, J. Meng, P. Ring, and D. Peña Arteaga, Phys. Rev. C **79**, 044312 (2009).
[39] J. M. Yao, J. Meng, P. Ring, and D. Vretenar, Phys. Rev. C **81**, 044311 (2010).
[40] T. R. Rodríguez and J. L. Egido, Phys. Rev. C **81**, 064323 (2010).
[41] J. M. Yao, H. Mei, H. Chen, J. Meng, P. Ring, and D. Vretenar, Phys. Rev. C **83**, 014308 (2011).
[42] J. M. Yao, J. Meng, P. Ring, Z. X. Li, Z. P. Li, and K. Hagino, Phys. Rev. C **84**, 024306 (2011).
[43] T. R. Rodríguez and J. L. Egido, Phys. Rev. C **84**, 051307 (2011).
[44] T. R. Rodríguez and J. L. Egido, Phys. Lett. B **705**, 255 (2011).
[45] J. Libert, M. Girod, and J.-P. Delaroche, Phys. Rev. C **60**, 054301 (1999).
[46] L. Próchniak, P. Quentin, D. Samsoen, and J. Libert, Nucl. Phys. A **730**, 59 (2004).
[47] T. Nikšić, Z. P. Li, D. Vretenar, L. Prochniak, J. Meng, and P. Ring, Phys. Rev. C **79**, 034303 (2009).
[48] Z. P. Li, T. Nikšić, D. Vretenar, J. Meng, G. A. Lalazissis, and P. Ring, Phys. Rev. C **79**, 054301 (2009).
[49] T. Nikšić, D. Vretenar, and P. Ring, Prog. Part. Nucl. Phys. **66**, 519 (2011).
[50] J. M. Yao, Z. P. Li, K. Hagino *et al.*, Nucl. Phys. A **868**, 12 (2011).
[51] J.-P. Delaroche, M. Girod, J. Libert *et al.*, Phys. Rev. C **81**, 014303 (2010); [http://www-phynu.cea.fr/science_en_ligne/carte_potentiels_microscopiques/tables/HFB-5DCH-table.htm].
[52] L. Próchniak, K. Zajac, K. Pomorski *et al.*, Nucl. Phys. A **648**, 181 (1999).
[53] P. W. Zhao, Z. P. Li, J. M. Yao, and J. Meng, Phys. Rev. C **82**, 054319 (2010).
[54] Y. Tian and Z. Y. Ma, and P. Ring, Phys. Lett. B **676**, 44 (2009).
[55] T. Nikšić, P. Ring, D. Vretenar, Y. Tian, and Z. Y. Ma, Phys. Rev. C **81**, 054318 (2010).
[56] E. Chabanat, P. Bonche, P. Haensel, J. Meyer, and R. Schaeffer, Nucl. Phys. A **635**, 231 (1998); **643**, 441(E) (1998).
[57] C. Rigollet, P. Bonche, H. Flocard, and P.-H. Heenen, Phys. Rev. C **59**, 3120 (1999).
[58] D. R. Inglis, Phys. Rev. **103**, 1786 (1956).
[59] S. T. Belyaev, Nucl. Phys. **24**, 322 (1961).
[60] M. Girod and B. Grammaticos, Nucl. Phys. A **330**, 40 (1979).
[61] P. Bonche, H. Flocard, and P.-H. Heenen, Comput. Phys. Commun. **171**, 49 (2005).
[62] National Nuclear Data Center, Brookhaven National Laboratory; [http://www.nndc.bnl.gov/index.jsp].
[63] M. Bender, G. F. Bertsch, and P.-H. Heenen, Phys. Rev. C **73**, 034322 (2006).
[64] F. Buchinger, E. B. Ramsay, E. Arnold *et al.*, Phys. Rev. C **41**, 2883 (1990).
[65] P. Campbell, H. L. Thayer, J. Billowes *et al.*, Phys. Rev. Lett. **89**, 082501 (2002).
[66] T. Kibédi and R. H. Spear, At. Data Nucl. Data Tables **89**, 77 (2005).
[67] [http://ie.lbl.gov/TOI2003/GammaSearch.asp].
[68] K. Heyde and J. L. Wood, Rev. Mod. Phys. **83**, 1467 (2011).
[69] [http://www-phynu.cea.fr/science_en_ligne/carte_potentiels_microscopiques/carte_potentiel_nucleaire.htm].